arXiv:1704.08519v1 [cond-mat.mtrl-sci] 27 Apr 2017

Breakdown of Polarons in Conducting Polymers at Device Field Strengths

M. R. Mahani,[*,†] A. Mirsakiyeva,[†] and Anna Delin[*,†,‡,¶]

†*Department of Applied Physics, School of Engineering Sciences, KTH Royal Institute of Technology, Electrum 229, SE-16440 Kista, Sweden*

‡*Department of Physics and Astronomy, Materials Theory Division, Uppsala University, Box 516, SE-75120 Uppsala, Sweden*

¶*Swedish e-Science Research Center (SeRC), KTH Royal Institute of Technology, SE-10044 Stockholm, Sweden*

E-mail: mrmahani@kth.se; annadel@kth.se

Abstract

Conducting polymers have become standard engineering materials, used in many electronic devices. Despite this, there is a lack of understanding of the microscopic origin of the conducting properties, especially at realistic device field strengths. We present simulations of doped poly(p-phenylene) (PPP) using a Su-Schrieffer-Heeger (SSH) tight-binding model, with the electric field included in the Hamiltonian through a time-dependent vector potential via Peierls substitution of the phase factor. We find that polarons typically break down within less than a picosecond after the field has been switched on, already for electric fields as low as around 1.6 mV/Å. This is a field strength common in many flexible organic electronic devices. Our results challenge the relevance of the polaron as charge carrier in conducting polymers for a wide range of applications.

Introduction

Conducting polymers have emerged as important materials for a number of very diverse applications such as, e.g., fuel cells, field effect transistors, organic light-emitting diodes (OLED), solar cells, computer displays, thermoelectric films, and in microsurgical tools.[1–6] Materials made from conducting polymers have numerous engineering-friendly properties – they are often easily synthesised, air stable, solution processable, flexible, and environmentally friendly. In several of the applications mentioned above, the charge transport properties are of central importance.[7–9] Charge transport, and charge carrier mobility in particular, is one of the fundamental physical processes that determine device performance. Considering how widely spread organic conductors are today in society – many people now use touch screens every day – the understanding of these charge carriers is surprisingly schematic, and existing models in use claim different physical origins of observed features.[10] Improved insight into the underlying physical processes is vital for improving device performance. Due to the large electron-phonon coupling in these one-dimensional systems, charge is thought to

be transported mainly in the form of polarons and (possibly) bipolarons, in which trapped charges self-localise together with an associated structural distortion. The dynamics of these charge carriers is complex and depends on, e.g., temperature, electric field, disorder, and system dimensionality.[11–15]

Here, we investigate theoretically charge transport as a function of electric field strength in the conducting polymer poly(p-phenylene) (PPP), also known as poly(1,4-phenylene). PPP was discovered in 1979[16] and is recognised as a useful high-performance polymer due to its thermal[17] and chemical[16] stability and its electrical and optoelectronic properties.[18–20] PPP has a very simple structure consisting of interconnected phenyl rings and therefore also serves as an archetypal example of a conducting polymer. PPP can also be viewed as an ultrathin graphene nanoribbon. From a theoretical perspective, a lot of work on fundamental aspects of charge transport in conducting polymers have been performed on polyacetylene[12–14,21,22] (PA).

The present investigations employ a generalization of the Su-Schrieffer-Heeger (SSH) Hamiltonian,[23–27] with an electric field introduced through a time-dependent vector potential.[28] Additional complexity and various interactions not included in this model are certainly present in real conjugated polymer systems. Though the size and morphology of polymer films in real devices is more complex than what is presented in this work (a single chain), a bottom-up approach is of special interest for understanding the underlying physical processes, determining the relation between the motion of the excitations and the electric field strength.

In devices made from conducting polymers, the strength of the applied electric field varies depending on the type of device. In thermoelectric applications, the field is of the order of μV/Å,[29] whereas in optoelectronic devices, field strenghts of typically a few mV/Å are common.[12,30–34]We have used these experimental values as a guideline in the present work. Specifically, we address field strengths in the range 1 μV/Å– 5 mV/Å. Our results indicate that polarons break down already at very moderate field strengths, common in

devices. Also the bipolarons show significant instability in the upper range of the addressed electric field strengths. However, we would like to emphasize that our conclusions are drawn from the linear isolated chain. A chain which is not perfectly aligned with the electric field will of course feel a different electric field which would change the break-down value of the field. As regards the isolated chain approximation, hopping between chains seems to further lower the stability of polarons.[21]

Theoretical model and computational details

The system addressed throughout this work is a PPP polymer consisting of 20 six-membered rings with periodic boundary conditions. To describe the effect of an electric field on the fundamental excitations in a doped polymer, we study the time evolution of the Hamiltonian

$$\begin{aligned} H_{\mathrm{SSH}} &= H_{\mathrm{el}} + H_{\mathrm{latt}}, \\ H_{\mathrm{el}} &= -\sum_n (t_0 - \alpha(u_{n+1} - u_n))(e^{i\gamma A} c_n^\dagger c_{n+1} + e^{-i\gamma A} c_{n+1}^\dagger c_n), \\ H_{\mathrm{latt}} &= \frac{1}{2}\sum_n K(u_{n+1} - u_n)^2 + \frac{1}{2}\sum_n M\dot{u}_n^2, \end{aligned} \tag{1}$$

which is a generalization of the original SSH Hamiltonian to account for the presence of an electric field.[28] In the above Hamiltonian, H_{el} is the electronic part and H_{latt} is the lattice part. H_{el} contains, in addition to hopping terms, the electron-phonon coupling terms. The parameter t_0 is the hopping integral between nearest-neighbor carbon sites, α is the electron-phonon coupling constant for the π electrons, u_n is the displacement of the n-th CH group[35] from its equilibrium position, $c_n^\dagger$ (c_n) is the creation (annihilation) operator for a π electron on the n-th site, K is the elastic constant associated with the σ bonds and M is the mass of the CH group.

The electric field is introduced in terms of a time-dependent vector potential, A, via Peierls substitution of the phase factor.[28,36] The parameter γ is defined as $\gamma = ea/\hbar c$ with

e, a, c being the absolute value of the electronic charge, the lattice constant and the speed of light, respectively. The electric field, then, is given by the time derivative of the vector potential, i.e. $E = -(1/c)\partial A/\partial t$.

We use periodic boundary conditions to avoid end-point effects. This also allows us to study the dynamics of the excitations for a longer period of time, without having to use an unnecessarily large system. The periodic boundary conditions implies that the position of the polaron (bipolaron), after it forms, can be anywhere along the chain, depending on the initial conditions. If one removes the periodic boundary conditions, the polaron (bipolaron) localised in the middle of the chain has the lowest ground state energy.[37]

A time dependent electric field uniform in space can be described with a vector potential that is independent of the space coordinates (a scalar potential describing the same electric field will not have this property). Therefore, introducing the electric field through a vector potential in the form of a complex phase factor to the phase integral is compatible with periodic boundary conditions.

In our simulations, we have set the parameters appearing in the Hamiltonian to the following values: $t_0 = 2.5\,\mathrm{eV}$, $K = 21\,\mathrm{eV\AA^{-2}}$, $\alpha = 4.1\,\mathrm{eV\AA^{-1}}$, $a = 1.22\,\mathrm{\AA}$ and $M = 1349.14\,\mathrm{eVfs^2\AA^{-2}}$. These values are the same as those commonly used for polyacetylene (PA).[28] Our choice is motivated by the fact that the backbone of PPP is essentially identical to that of PA. Additionally, this set of parameters not only reproduce the electronic properties of PPP in zero field (measured energy gaps in short PPP oligomers[38,39]), but it also allows us to compare our results with those of PA. The PA structure using the same tight-binding Model has the energy level and band gap according to Ref.[23,25,40], while using the same set of parameters for PPP, as first order of approximation, would give a different electronic structure and band gap in our calculations.

In principle, the band gap can be fine-tuned by introducing additional parameters for the electron-phonon coupling in aromatic rings.[39] However, such fine-tuning can be expected to have a relatively small effect on the overall charge carrier dynamics and therefore we have

not included them in the present work. More elaborate models – with, e.g., the electron-electron interaction included together with the already mentioned additional parameters for the electron-phonon coupling in aromatic rings – will be the subject of future work.

The static initial-state geometry of the charged polymer is determined with the electric field set to zero, allowing polarons and bipolarons to form. By minimizing the ground state total energy of the system using the Hellman-Feynman force theorem within the adiabatic approximation with zero electric field, one arrives at

$$u_n = \frac{1}{2}(u_{n+1} + u_{n-1}) + \frac{2\alpha}{K}\sum_k{}' (\psi_k^*(n)\psi_k(n+1) - \psi_k^*(n-1)\psi_k(n)), \tag{2}$$

where $\psi_k(n)$ is an eigenfunction at site n. The sum is over all occupied states. The static initial-state geometry is then computed self-consistently by starting with an initial guess for the displacements, and then repeatedly applying equation (2) until convergence, using the constraint that the total length of the system is constant.[28]

In order to study the dynamics of the geometry-optimised charged excitations, we switch on the electric field at $t = 0$ and linearly raise it to its maximum during the first 50 fs of the simulation. With this gradual onset of the electric field, we avoid disturbances due to sudden switching.[41] In principle, switching on the electric field before optimizing the doped system could be used to address processes in which the electrons are, for example, hopping from another chain into the system. However, there are studies for polyacetylene showing that applying a field above a certain value before optimizing the structure leads to nonspecific patterns rather than forming polarons or bipolarons.[42] Such transport processes are deemed out of scope in the present work.

The evolution of the system is computed by solving the time-dependent Schrödinger

equation

$$i\hbar\frac{\partial\psi(n,t)}{\partial t} = (-t_0 + \alpha(u_{n+1} - u_n))e^{i\gamma A}\psi(n+1,t) + (-t_0 + \alpha(u_n - u_{n-1}))e^{-i\gamma A}\psi(n-1,t), \quad (3)$$

and the equation of motion for the lattice displacement

$$M\ddot{u}_n(t) = F_n(t) = -K(2u_n - u_{n+1} - u_{n-1}) + \alpha\sum_k{}' e^{i\gamma A}(\psi_k^*(n)\psi_k(n+1) - \psi_k^*(n-1)\psi_k(n)) + H.c. \quad (4)$$

simultaneously. In the equation of motion, equation (4), the forces $F_n(t)$ are derived from the total potential, i.e. the sum of the electronic potential and the lattice harmonic potential. The coupled differential equations are solved numerically using the procedure of Ono and coworkers,[28] briefly outlined below. The solutions of the time-dependent Schrödinger equation are

$$\psi_k(t) = Te^{-i/\hbar\int_0^t \hat{h}(t')dt'}\psi_k(0), \quad (5)$$

where $\hat{h}(t)$ is the single particle Hamiltonian and T the time ordering operator. To compute this expression numerically, time needs to be discretised. We choose the time step Δt to be 0.025 fs, which is very small on the scale of the bare phonon frequency $\omega_Q = \sqrt{4K/M}$ of the system. With this choice, the variation of the Hamiltonian within a time step can be assumed to be negligible, and the electronic wave function can be written

$$\psi_k(t_{j+1}) = e^{-i\hat{h}(t_j)\Delta t/\hbar}\psi_k(t_j). \quad (6)$$

By expanding the electronic wave function in terms of the eigenfunction (ϕ_l) and eigenvalues (ϵ_l) of the single-particle Hamiltonian $\hat{h}(t)$ at each time step, the wave function becomes

$$\psi_k(n,t_{j+1}) = \sum_l \left[\sum_p \phi_l^*(p)\psi_k(p,t_j) \right] e^{-i\epsilon_l \Delta t/\hbar} \phi_l(n). \tag{7}$$

This set of coupled equations can be numerically integrated using the following algorithm:

$$u_n(t_{j+1}) = u_n(t_j) + \dot{u}_n(t_j)\Delta t, \qquad \dot{u}_n(t_{j+1}) = \dot{u}_n(t_j) + \frac{F_n(t_j)}{M}\Delta t \ , \tag{8}$$

resulting in the pertinent time-dependent electronic wave functions.

To analyze the motion of the excitations, the polaron and bipolaron positions and velocities need to be computed. The position of the excitation is defined by considering the center of mass x_c for the excess charge density ρ_n, taking the periodic boundary conditions into account.[28] Thus,

$$x_c = \begin{cases} N\theta/2\pi, & \langle \cos\theta_n \rangle \geq 0 \quad \text{and} \quad \langle \sin\theta_n \rangle \geq 0, \\ N(\theta+\pi)/2\pi, & \langle \cos\theta_n \rangle \leq 0, \\ N(\theta+2\pi)/2\pi, & \text{otherwise}, \end{cases} \tag{9}$$

where

$$\langle \cos\theta_n \rangle = \sum_n \rho_n \cos(2\pi n/N), \quad \langle \sin\theta_n \rangle = \sum_n \rho_n \sin(2\pi n/N),$$
$$\theta = \arctan\left(\frac{\langle \sin\theta_n \rangle}{\langle \cos\theta_n \rangle} \right),$$

and the excess charge density ρ_n is given by

$$\rho_n(t) = \sum_k{}' \mid \psi_k(n,t) \mid^2 -1. \tag{10}$$

From the computed x_c, the velocity is calculated as an average velocity over 400 time steps

according to

$$v(t_j) = \frac{x_c(t_j) - x_c(t_j - 400\Delta t)}{400\Delta t}. \quad (11)$$

As already mentioned, our model does not include the effects of electron-electron correlations. These effects can be implemented through the on-site and off-site Hubbard terms, similar to what has been done for PA.[43–45] Alternatively, the density matrix renormalization group (DMRG) could be used for addressing the interactions.[46]

Results and discussion

Our simulations reveal that the behavior of the charge carriers depend sensitively on the electric field strength. There is a weak field regime with well-localised polaronic sonic or supersonic states, and a strong field regime, where the charge and lattice degrees of freedom decouple. In Table 1 we summarise our computed critical field strengths. Interestingly, we

Table 1: Summary of critical field strengths for polarons (PPP^+) and bipolarons (PPP^{2+}) in PPP. The electric field strengths are given in mV/Å.

	PPP^+	PPP^{2+}
sonic – supersonic	0.15-0.155	0.6-0.65
supersonic – breakdown	1.4-1.6	3.2-3.3

find that polarons break down already at around 1.6 mV/Å. This is a field strength present in many flexible electronics devices. Below, we describe the polaron and bipolaron properties as a function of field strength in more detail. We begin with the static regime, i.e. when the electric field is zero. The static regime is the starting point in all our simulations.

Schematic diagrams of the pertinent energy levels in the system are shown in Fig. 1a. The leftmost panel shows the neutral case (PPP^0). Here, each level is doubly occupied up to the Fermi energy. H stands for the highest occupied level, and L for the lowest unoccupied level. The middle panel shows the singly doped case (PPP^+), in which one electron has been removed. Two polaronic levels appear in the gap, of which the lowest one is singly occupied and the higher one unoccupied. Finally, the rightmost panel shows the bipolaronic

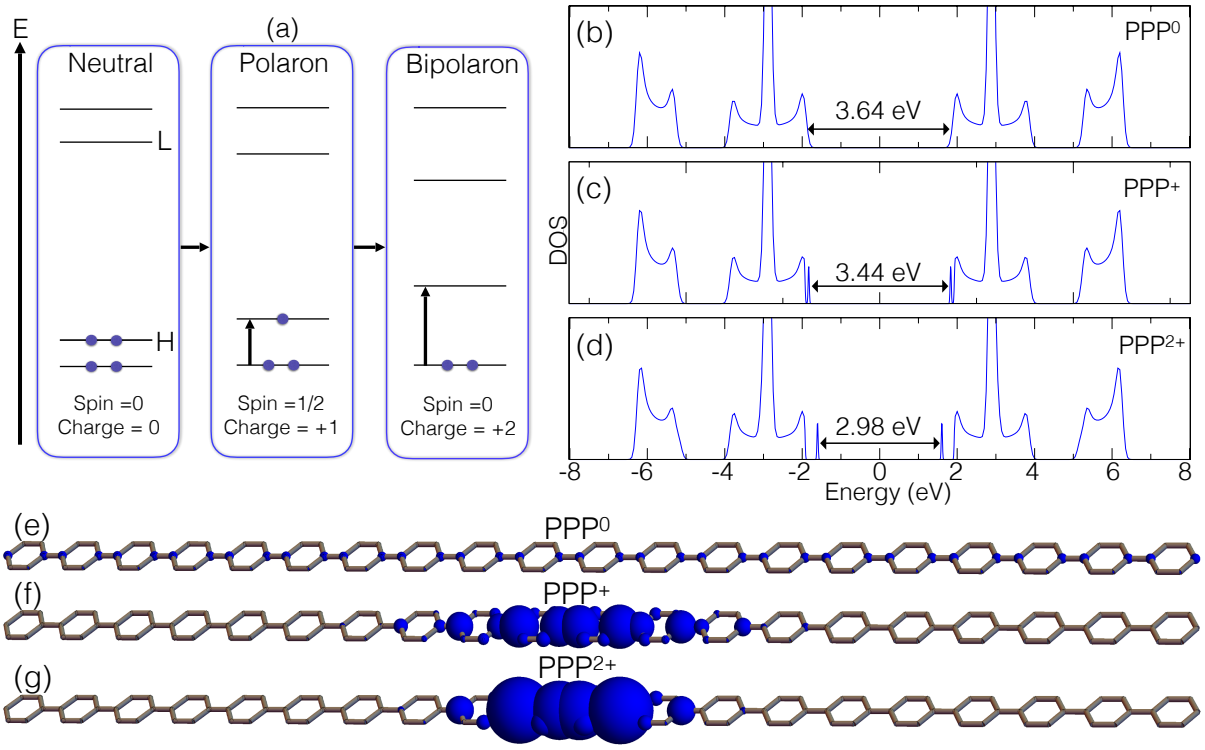

Figure 1: (Colour online) Level structures, densities of states (DOS) and charge distributions of neutral and p-doped PPP. (a) The level structures in the gap for three cases. (b)–(d) DOS of neutral (PPP^0), singly charged (PPP^+) and doubly charged PPP (PPP^{2+}), respectively. (e)–(g) Visualization of the charge density corresponding to the highest occupied level (neutral case) and lowest in-gap (bi)polaronic levels, respectively. The radius of each blue sphere is proportional to the wave function amplitude on that site. The order parameter indicating the bond change coincides with the area of the polymer that the charge is localised to. The Fermi level for the neutral case is at the top of the valence band, where the DOS has finite value below the zero energy.

case (PPP^{2+}). Here, two electrons have been removed. Compared to the polaronic case, the emerging levels appear deeper in the gap and they are both unoccupied.

The calculated density of states (DOS) of PPP^0, PPP^+ and PPP^{2+} polymers are shown in Fig. 1b-d, respectively. We see that the energy gaps and the shapes of the DOS for PPP^0 and PPP^+ are the same as in previous studies.[39] For the bipolaronic case, we find that the gap narrows to 2.98 eV while it is 3.44 eV for the singly charged case. Compared to the polaronic state, the bipolaron is more localised and deeper in the gap.

In Fig. 1e-g, the charge densities of the three cases are visualised. For PPP^0, we show the charge density of the highest occupied level, whereas for PPP^+ and PPP^{2+}, we show the lowest in-gap level which represents the (bi)polaronic states. The radii of the blue spheres at each site correspond to the charge distribution of this level at that site. We see that the polaron extends over about six rings, whereas the bipolaron is about four rings wide. Our calculations thus confirm that the wave function of the bipolaron is more localised than that of the polaron, which agrees with the observed deeper gap states in the DOS (Fig. 1d).

It is relevant to compare our results with a recent DFT study[10] where a density functional with pure Hartree-Fock exchange in the long-range and pure Perdew-Burke-Ernzerhof (PBE) exchange in the short range was employed. In these calculations, the dihedral angles were also optimised, giving an interring rotation of about 39° in the neutral polymer, and an oscillating interring rotation ranging from around 22° to 50° inside the polaron. The long-range exchange tail allows a polaron to form. At the same time, shifts of the energy levels in and around the polaron due to the excess charge is accounted for. Due to these shifts, the gap states are no longer symmetrically positioned within the gap. The band gap in the neutral polymer in the DFT-based computation[10] appears to be about 6 eV, which is significantly larger than the band gap in our model (3.64 eV), what experimental data for short isolated oligomers suggest,[38,39] as well as what recent *GW* computations find (3.95 eV).[47] The discrepancy between the typical experimental value of the gap in PPP (2.8 eV) and the band gap in our model (3.64 eV) warrants a few comments. The value 2.8 eV refers to the optical

gap, and is determined from ultra-violet (UV) spectral measurements on a PPP film,[48] i.e., for PPP molecules not in vacuum. Interestingly, *GW* calculations give that when a PPP chain is adsorbed on graphene at a distance of 4.0 Å, the gap is renormalized from 3.95 eV to 2.7 eV.[47] Thus, it appears that the environment heavily influences the value of the gap, and calculations for an isolated PPP chain cannot be compared directly with measurements on a PPP film, solution, or matrix. The optical spectrum of a conjugated polymer typically also has a wide absorption band due to intrinsic disorder, which leads to significant uncertainty in the determination of the optical band gap. Furthermore, the electronic gap, which is the gap our model refers to, is very difficult to measure directly and is larger than the optical gap due to excitonic interaction. Finally, we also mention that in our model, the interring dihedral angles are assumed to be zero in all cases, which may somewhat affect the band gaps.

The visible changes in the bond lengths after doping the system in the mentioned DFT study[10] covers approximately six rings which compares well with our results for the polaron. In the DFT study, the bipolaron could not be stabilised, due to Coulomb repulsion. In general, including Coulomb repulsion in the SSH model is expected to weaken the bipolaronic state or cause it to become unstable, depending on the Coulomb interaction parameters.

We now turn to the real time dynamics of polarons as a function of electric field strength. In Fig. 2 we show the time evolution of the lattice distortions, excess charge and polaronic-state wave function of p-doped PPP after applying 0.25, 2 and 5 mV/Å electric fields. The weak field is chosen such that the charge and lattice distortions are coupled throughout the simulation time (up to 2 ps). The intermediate field is above the threshold for which the charge and the lattice distortions decouple. Finally, the strong field demonstrates how the polaron breaks down already at a very early stage in the simulation, just $t = 49$ fs after initialisation.

Figs. 2a and 2b show the time evolution of the displacements, $y_n = u_{n+1} - u_n$, and the excess charge $\rho_n(t)$, defined in equation (10), for a polaron in a 0.25 mV/Å electric field.

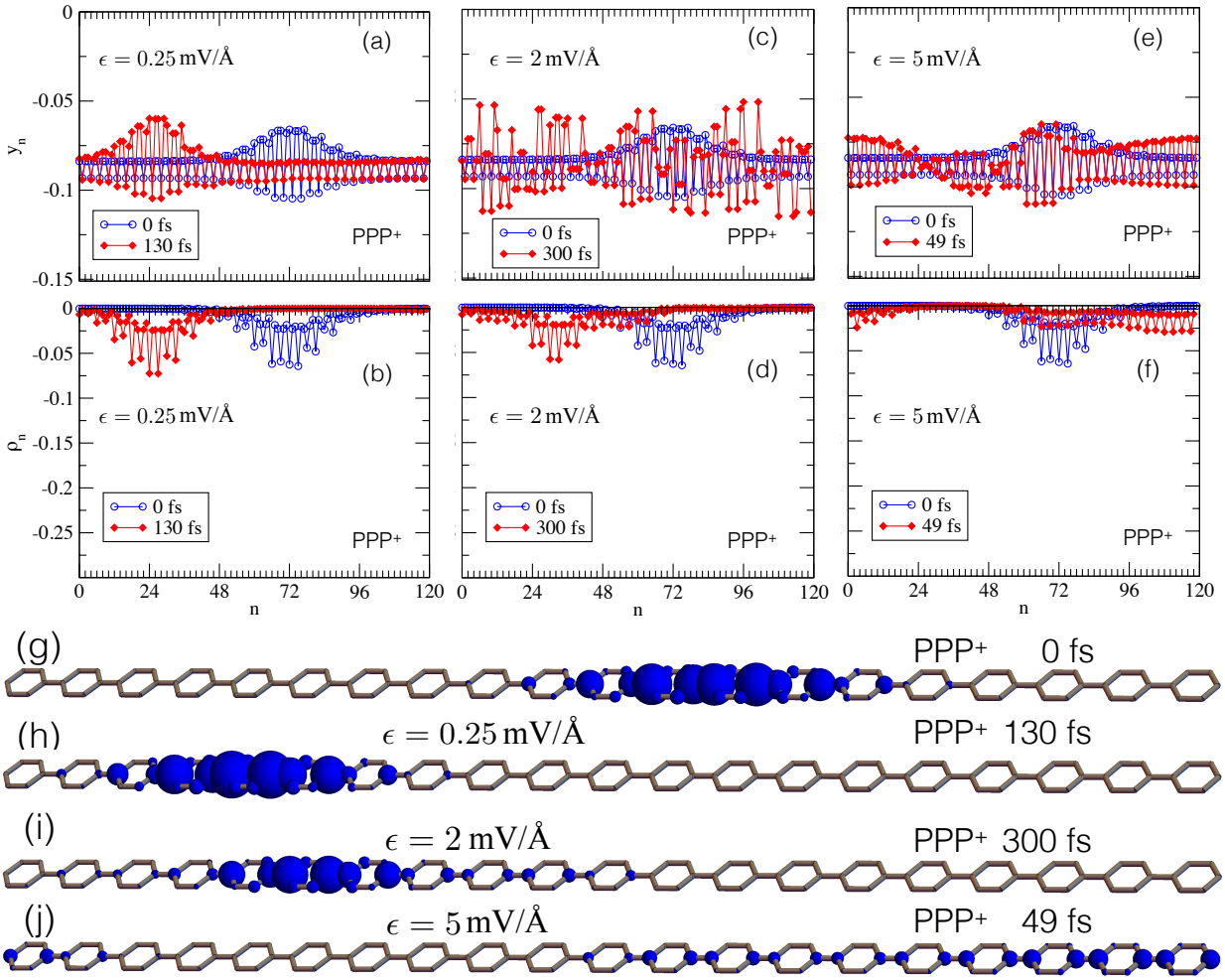

Figure 2: (Colour online) The time evolution of the lattice distortion, excess charge, and polaronic-state wave function of p-doped PPP after applying 0.25, 2 and 5 mV/Å electric fields. (a) and (b): The evolution of the lattice distortion and the excess charge in 0.25 mV/Å electric field, respectively. (c), (d) and (e), (f): Similar to (a), (b) but in 2 and 5 mV/Å fields, respectively. The blue line with circle is for $t = 0$ and the red line with filled-diamond is for t. (g) The polaron wave function at $t = 0$ for all electric fields. The electric field is switched on at $t = 0$ and gradually ramped up during the first 50 fs of the simulation. The size of the blue spheres in panels g-j is according to Fig. 1. (h)-(j) The evolution of the polaron wave function in 0.25, 2 and 5 mV/Å electric fields at different times.

The blue circles (red filled diamonds) show a snapshot of the calculated quantity at $t = 0$ ($t = 130$ fs). After 130 fs, the positively charged polaron has moved to the end of the chain in the direction of the applied field. Clearly, the displacement and the excess charge are coupled to one another and move as one entity. This remains the case for the entire simulation time, up to 2 ps.

Figs. 2e and 2f are similar to Figs. 2a and 2b but for an electric field of 5 mV/Å. In this rather strong electric field the polaron charge cloud decouples from the lattice deformations. As one can see from panels 2e and 2f, after only 49 fs the excess charge density is spread through the polymer and is thus completely detached from the lattice deformations. For electric fields strengths just above the stability threshold, here examplified iwth the field strengths 2 mV/Å, the polaron breaks down in a similar way, but it takes longer time. This is illustrated in Figs. 2c-d. For long simulation times, we observe that polarons may occasionally reform and break down again.

Figs. 2g-j illustrate the corresponding eigenstates, showing the distribution of the charges on the atomic sites and their movements after applying the electric field. In our nearest-neighbor tight-binding model, the electric field forces the charge to hop between the nearest sites along the direction of the field. The size of the sphere around each site is proportional to the wave function amplitudes of that site at a given time. The excitations in panels 2h (weak field), continue to move as an entity along the chain even for very long simulation times. This picture does not hold for 2 and 5 mV/Å fields, where the polaron dissociates. This is clear from panels 2i, where the polaron after about 300 fs under 2 mV/Å electric field is delocalized. The localized charge spreads quickly (within only 49 fs) over a large part of the chain in 5 mV/Å electric field. Similar to the charge dynamics in polyacetylene (PA),[49] we observe charge induced lattice deformation at later times after the initital polaron breakdown.

Fig. 3 exemplifies the polaron velocity at three different fields strengths: 1 μV/Å, 0.1 mV/Å, and 0.5 mV/Å. For all these field strengths the charge and the lattice are not decoupled and

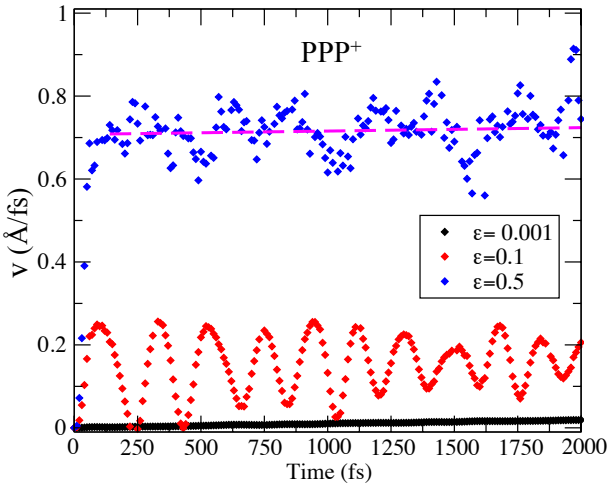

Figure 3: (Colour online) The polaron velocity as a function of time for three representative electric field strengths ϵ in units of mV/Å. The magenta dashed line is a guide for the eye.

therefore the definition of the velocity (equation (11)) holds. As one can deduce from Fig. 3, the polaron velocity depends on the strength of the electric field in a highly nonlinear way. For the very weak field 1 μV/Å, which is of the same order as the electric field in a thermoelectric device, the pumped energy via electric field does not move the polaron along the polymer chain, throughout our simulation (up to 2 ps). When the field strength is increased but kept in the sonic regime, we observe significant oscillations in the velocity of the polaron, i.e. the polaron reaches a maximum speed and slows down – in fact almost stops – repeatedly. This regime is the result of coupling between charge and the acoustic phonons. For other fields in this regime, the velocities oscillate approximately around the same saturation velocity (not shown).

Finally, in the supersonic regime, where the charge instead couples to the optical phonons,[37] the polaron velocity reaches a higher saturation value compared to sonic regime. In our simulations, the saturation velocity is attained after about 130 fs. After this short period of time, the energy pumped into the system by the electric field dissipates to the lattice vibrations at the same rate, so that the acceleration of the polaron becomes zero. The dissipation is continuous due to the classical description of the lattice in the SSH model.

The saturation velocity in the supersonic regime is about three times larger (around

0.7 Å/fs) than the maximum velocity in the sonic regime (around 0.25 Å/fs). For other fields in the supersonic regime, the saturation velocity is similar to the one shown. The corresponding velocities for PA[37] are about 0.45 Å/fs in the supersonic regime and 0.13 Å/fs in the sonic regime. Since the sound velocity, defined as $v_s = (a/2)\sqrt{4K/M}$ within this model, is similar in PA and PPP (due to the use of the same set of parameters) we believe the difference originates from the different geometries of these two polymers. According to our simulations, the threshold electric field between the sonic and supersonic regimes lies between 0.15 mV/Å and 0.155 mV/Å. This is slightly larger than what has been theoretically predicted for PA (0.135 mV/Å–0.14 mV/Å).[37]

In addition, we have also calculated the potential, electronic, kinetic and total energy differences, i.e. the energy at time t subtracted by its counterpart at $t = 0$, of the system. Our calculations show that the total energy of the system is increasing with time. This is expected, since the system is not connected to any external heat bath. In the weak field regime, the potential energy $(1/2)\sum_n K(u_{n+1} - u_n)^2$ is in phase but with opposite sign to the electronic energy $\sum_l' \sum_k' C_{k,l}\epsilon_l$. Therefore, the energy pumped into the systems via the electric field goes through the electrons to the lattice. In other words, in the weak field regime the potential energy increases and the electronic energy decreases, whereas in the strong field the electronic energy increases.

We finally also briefly discuss our results for bipolarons. Studies for PA suggest that the exists a range of on-site Hubbard parameters[50] for which the bipolaronic state is more stable than two separate polarons. Therefore the bipolaronic state warrants consideration. In the present simulations, we neglect electron-electron correlations, as mentioned in the method section. Therefore, our bipolaron results may be considered as the limit of maximum coupling.

Fig. 4 shows the bipolaron dynamics for selected field strengths. In panels a and b, the lattice displacements and excess charge for PPP^{2+} in a weak field are shown. Compared to the polaron case, the displacements around the charge are localised on fewer sites and are

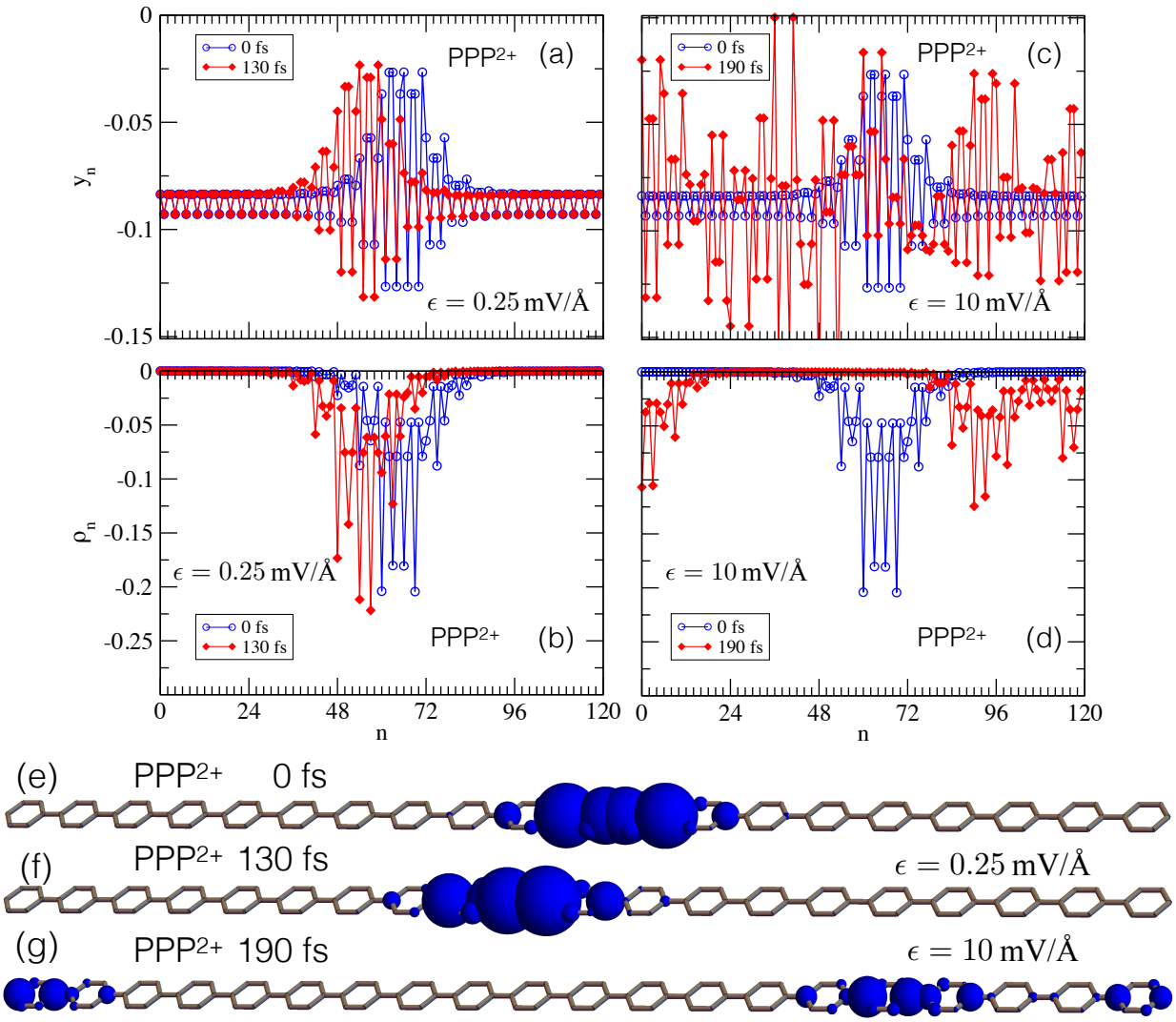

Figure 4: (Colour online) Similar to Figure 2 but for bipolaron. The time evolution of the lattice distortion, excess charge, and bipolaronic-state wave function of p-doped PPP after applying 0.25 and 10 mV/Å electric fields. (a) and (b): The evolution of the lattice distortion and the excess charge in 0.25 mV/Å electric field, (c) and (d): The evolution of the lattice distortion and the excess charge in 10 mV/Å electric field. (e)-(f) The evolution of the bipolaron wave function in 0.25 mV/Å electric field for two different times. (g) The snapshot of the bipolaron wave function in 10 mV/Å electric field. The blue line with circle is for $t = 0$ and the red line with filled-diamond is for t. The size of the blue spheres in panels e-h is according to Fig. 1. The electric field is switched on at $t = 0$ and gradually ramped up during the first 50 fs of the simulation.

greater in magnitude.

Figs. 4c-d illustrate bipolaron breakdown in a strong electric field (10 mV/Å). Here, the bipolaron dissociates after about 190 fs. Compared to the polaron case, a significantly stronger electric field is needed to decouple the charge from the lattice distortions. However, if we were to include electron-electron correlations in the model, the bipolaronic state would become less stable, and the break-down field would in any case be lower than in the present calculation.

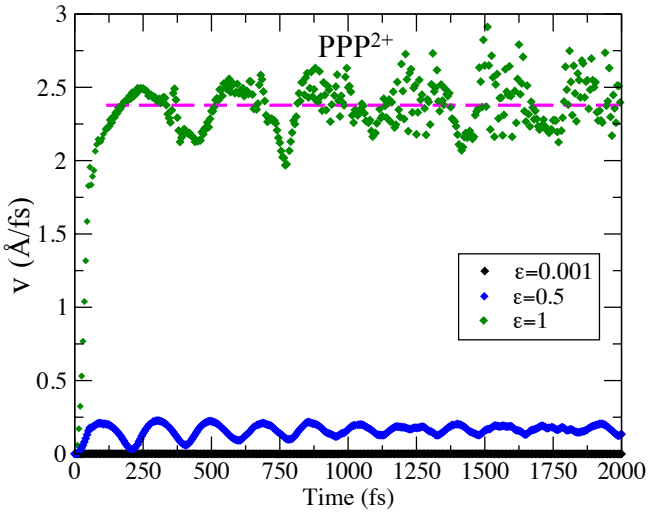

Figure 5: (Colour online) The bipolaron velocity as a function of time for for three representative electric field strengths ϵ in units of mV/Å. The magenta dashed line is a guide for the eye.

The bipolaron velocity for three representative field strengths is shown in Fig. 5. Just as for the polaron, the bipolaron velocity oscillates in the sonic regime (blue dots). Some initial oscillations are also discernible in the supersonic regime (green dots). The bipolaron velocity in the supersonic regime is about three times higher than for polarons.

Conclusions

In conclusion, we have demonstrated that polarons in fact appear to be relatively unstable in an electric field. For normal device field strengths, we find that they quickly dissolve

and delocalize over the polymer. For electric field strengths just above the break-down field 1.6 mV/Å, the polarons occasionally localize and then dissolve again. The results are obtained by simulation of the SSH Hamiltonian for PPP, which is an archetypal conducting polymer. Also the bipolarons in our model break down at relatively moderate electric field strengths. The reliability of our model is ensured by comparing the PPP electronic structure for both the neutral and charged cases with available data. Our results challenge the common view that polarons are central for the charge transport in many types of devices based on conducting polymers. Polaronic states can be detected using a variety of techniques, e.g., time- and wavelength-resolved pump-probe measurements, Raman spectroelectrochemistry, single-molecule fluorescence spectroscopy (SMS), photoinduced absorption (PIA) spectroscopy, and electron spin resonance (ESR) spectroscopy. We hope that the results presented here will inspire additional such experiments, explicitly addressing how the signal is affected by an external electric field.

acknowledgement

We acknowledge financial support from Vetenskapsrådet (VR), The Royal Swedish Academy of Sciences (KVA), the Knut and Alice Wallenberg Foundation (KAW), Carl Tryggers Stiftelse (CTS), Swedish Energy Agency (STEM), and Swedish Foundation for Strategic Research (SSF). The computations were performed on resources provided by the Swedish National Infrastructure for Computing (SNIC) at the National Supercomputer Center (NSC), Linköping University, the PDC Centre for High Performance Computing (PDC-HPC), KTH, and the High Performance Computing Center North (HPC2N), Umeå University.

References

(1) Grätzel, M. Photoelectrochemical Cells. *Nature* **2001**, *414*, 338–344.

(2) Forrest, S. R. The Path to Ubiquitous and Low-Cost Organic Electronic Appliances on Plastic. *Nature* **2004**, *428*, 911–918.

(3) Heeger, A. J.; Kivelson, S.; Schrieffer, J.; Su, W.-P. Solitons in Conducting Polymers. *Reviews of Modern Physics* **1988**, *60*, 781.

(4) Gustafsson, G.; Cao, Y.; Treacy, G.; Klavetter, F.; Colaneri, N.; Heeger, A. Flexible Light-Emitting Diodes Made From Soluble Conducting Polymers. *Nature* **1992**, *357*, 477–479.

(5) Balint, R.; Cassidy, N. J.; Cartmell, S. H. Conductive Polymers: Towards a Smart Biomaterial for Tissue Engineering. *Acta biomaterialia* **2014**, *10*, 2341–2353.

(6) Vasseur, G.; Fagot-Revurat, Y.; Sicot, M.; Kierren, B.; Moreau, L.; Malterre, D.; Cardenas, L.; Galeotti, G.; Lipton-Duffin, J.; Rosei, F. et al. Quasi One-Dimensional Band Dispersion and Surface Metallization in Long-Range Ordered Polymeric Wires. *Nature communications* **2016**, *7*.

(7) Pandey, R. K.; Yadav, S. K.; Upadhyay, C.; Prakash, R.; Mishra, H. Surface Plasmon Coupled Metal Enhanced Spectral and Charge Transport Properties of Poly(3,3-dialkylquarterthiophene) Langmuir Schaefer Films. *Nanoscale* **2015**, *7*, 6083–6092.

(8) Chen, J.; Shao, M.; Xiao, K.; Rondinone, A. J.; Loo, Y.-L.; Kent, P. R.; Sumpter, B. G.; Li, D.; Keum, J. K.; Diemer, P. J. et al. Solvent-Type-Dependent Polymorphism and Charge Transport in a Long Fused-Ring Organic Semiconductor. *Nanoscale* **2014**, *6*, 449–456.

(9) Adhikary, P.; Venkatesan, S.; Adhikari, N.; Maharjan, P. P.; Adebanjo, O.; Chen, J.; Qiao, Q. Enhanced Charge Transport and Photovoltaic Performance of PBDTTT-CT/PC 70 BM Solar Cells via UV–Ozone Treatment. *Nanoscale* **2013**, *5*, 10007–10013.

(10) Heimel, G. The Optical Signature of Charges in Conjugated Polymers. *ACS central science* **2016**,

(11) Junior, L. A. R.; Stafström, S. Polaron Stability in Molecular Semiconductors: Theoretical Insight into the Impact of the Temperature, Electric Field and the System Dimensionality. *Physical Chemistry Chemical Physics* **2015**, *17*, 8973–8982.

(12) Ribeiro, L. A.; da Cunha, W. F.; de Oliveria Neto, P. H.; Gargano, R.; e Silva, G. M. Effects of Temperature and Electric Field Induced Phase Transitions on the Dynamics of Polarons and Bipolarons. *New Journal of Chemistry* **2013**, *37*, 2829–2836.

(13) da Silva, M. V. A.; de Oliveira Neto, P. H.; da Cunha, W. F.; Gargano, R.; e Silva, G. M. Supersonic Quasi-Particles Dynamics in Organic Semiconductors. *Chemical Physics Letters* **2012**, *550*, 146–149.

(14) Johansson, A. A.; Stafström, S. Nonadiabatic Simulations of Polaron Dynamics. *Physical Review B* **2004**, *69*, 235205.

(15) Zhang, S. The Microscopic Origin of the Doping Limits in Semiconductors and Wide-Gap Materials and Recent Developments in Overcoming these Limits: a Review. *Journal of Physics: Condensed Matter* **2002**, *14*, R881.

(16) Ivory, D.; Miller, G.; Sowa, J.; Shacklette, L.; Chance, R.; Baughman, R. Highly Conducting Charge-Transfer Complexes of Poly(p-phenylene). *The Journal of Chemical Physics* **1979**, *71*, 1506–1507.

(17) Kovacic, P.; Jones, M. B. Dehydro Coupling of Aromatic Nuclei by Catalyst-Oxidant Systems: Poly(p-phenylene). *Chemical Reviews* **1987**, *87*, 357–379.

(18) Grem, G.; Leditzky, G.; Ullrich, B.; Leising, G. Realization of a Blue-Light-Emitting Device Using Poly(p-phenylene). *Advanced Materials* **1992**, *4*, 36–37.

(19) Grem, G.; Leditzky, G.; Ullrich, B.; Leising, G. Blue Electroluminescent Device Based on a Conjugated Polymer. *Synthetic metals* **1992**, *51*, 383–389.

(20) Grem, G.; Leising, G. Electroluminescence of "Wide-Bandgap" Chemically Tunable Cyclic Conjugated Polymers. *Synthetic metals* **1993**, *57*, 4105–4110.

(21) Johansson, Å.; Stafström, S. Polaron Dynamics in a System of Coupled Conjugated Polymer Chains. *Physical review letters* **2001**, *86*, 3602.

(22) Basko, D.; Conwell, E. Stationary Polaron Motion in a Polymer Chain at High Electric Fields. *Physical review letters* **2002**, *88*, 056401.

(23) Su, W.; Schrieffer, J.; Heeger, A. J. Solitons in Polyacetylene. *Physical Review Letters* **1979**, *42*, 1698.

(24) Su, W.; Schrieffer, J. Fractionally Charged Excitations in Charge-Density-Wave Systems with Commensurability 3. *Physical Review Letters* **1981**, *46*, 738.

(25) Su, W. P.; Schrieffer, J. R.; Heeger, A. J. Soliton Excitations in Polyacetylene. *Physical Review B* **1980**, *22*, 2099–2111.

(26) Takayama, H.; Lin-Liu, Y. R.; Maki, K. Continuum Model for Solitons in Polyacetylene. *Physical Review B* **1980**, *21*, 2388–2393.

(27) Su, W.; Schrieffer, J. Soliton Dynamics in Polyacetylene. *Proceedings of the National Academy of Sciences* **1980**, *77*, 5626–5629.

(28) Ono, Y.; Terai, A. Motion of Charged Soliton in Polyacetylene Due to Electric Field. *Journal of the Physical Society of Japan* **1990**, *59*, 2893–2904.

(29) Bubnova, O.; Berggren, M.; Crispin, X. Tuning the Thermoelectric Properties of Conducting Polymers in an Electrochemical Transistor. *Journal of the American Chemical Society* **2012**, *134*, 16456–16459.

(30) Lin, L.; Meng, H.; Shy, J.; Horng, S.; Yu, L.; Chen, C.; Liaw, H.; Huang, C.; Peng, K.; Chen, S. Triplet-To-Singlet Exciton Formation in Poly(p-phenylene-vinylene) Light-Emitting Diodes. *Physical review letters* **2003**, *90*, 036601.

(31) Gross, M.; Müller, D. C.; Nothofer, H.-G.; Scherf, U.; Neher, D.; Bräuchle, C.; Meerholz, K. Improving the Performance of Doped π-Conjugated Polymers for Use in Organic Light-Emitting Diodes. *Nature* **2000**, *405*, 661–665.

(32) Barth, S.; Müller, P.; Riel, H.; Seidler, P.; Riess, W.; Vestweber, H.; Bässler, H. Electron Mobility in Tris(8-hydroxy-quinoline) Aluminum Thin Films Determined via Transient Electroluminescence from Single- and Multilayer Organic Light-Emitting Diodes. *Journal of Applied physics* **2001**, *89*, 3711–3719.

(33) Yamamoto, H.; Wilkinson, J.; Long, J. P.; Bussman, K.; Christodoulides, J. A.; Kafafi, Z. H. Nanoscale Organic Light-Emitting Diodes. *Nano letters* **2005**, *5*, 2485–2488.

(34) Tutiŝ, E.; Berner, D.; Zuppiroli, L. Internal Electric Field and Charge Distribution in Multilayer Organic Light-Emitting Diodes. *Journal of applied physics* **2003**, *93*, 4594–4602.

(35) Of course, the carbon atoms linking together adjacent phenyl rings are not CH-groups, but for simplicity of the model this mass is assumed for all sites.

(36) Peierls, R. E. *Quantum Theory of Solids*; Oxford University Press, 1955.

(37) Johansson, A. A.; Stafström, S. Nonadiabatic Simulations of Polaron Dynamics. *Physical Review B* **2004**, *69*, 235205.

(38) Diaz, A.; Crowley, J.; Bargon, J.; Gardini, G.; Torrance, J. Electrooxidation of Aromatic Oligomers and Conducting Polymers. *Journal of Electroanalytical Chemistry and Interfacial Electrochemistry* **1981**, *121*, 355–361.

(39) Botelho, A. L.; Shin, Y.; Li, M.; Jiang, L.; Lin, X. Unified Hamiltonian for Conducting Polymers. *Journal of Physics: Condensed Matter* **2011**, *23*, 455501.

(40) Rossi, G. Minimum Total Energy Calculations for Conjugated Polymer Chains. *The Journal of chemical physics* **1991**, *94*, 4031–4041.

(41) Kuwabara, M.; Ono, Y.; Terai, A. Motion of Charged Soliton in Polyacetylene Due to Electric Field. II. Behavior of Width. *Journal of the Physical Society of Japan* **1991**, *60*, 1286–1293.

(42) Rakhmanova, S.; Conwell, E. Polaron Dissociation in Conducting Polymers by High Electric Fields. *Applied physics letters* **1999**, *75*, 1518–1520.

(43) Ozawa, T.; Ono, Y. Dynamics of an Acoustic Bipolaron in One-Dimensional Electron-Lattice Systems. *Journal of the Physical Society of Japan* **2000**, *69*, 1162–1169.

(44) Subbaswamy, K. R.; Grabowski, M. Bond Alternation, On-site Coulomb Correlations, and Solitons in Polyacetylene. *Physical Review B* **1981**, *24*, 2168–2173.

(45) Lin, X.; Li, J.; Först, C. J.; Yip, S. Multiple Self-Localized Electronic States in Trans-Polyacetylene. *Proceedings of the National Academy of Sciences* **2006**, *103*, 8943–8946.

(46) Jeckelmann, E.; White, S. R. Density-Matrix Renormalization-Group Study of the Polaron problem in the Holstein Model. *Physical Review B* **1998**, *57*, 6376.

(47) Puschnig, P.; Amiri, P.; Draxl, C. Band Renormalization of a Polymer Physisorbed on Graphene Investigated by Many-Body Perturbation Theory. *Physical Review B* **2012**, *86*, 085107.

(48) Eckhardt, H.; Shacklette, L.; Jen, K.; Elsenbaumer, R. The Electronic and Electrochemical Properties of Poly(phenylene vinylenes) and Poly(thienylene vinylenes): An Experimental and Theoretical Study. *The Journal of Chemical Physics* **1989**, *91*, 1303–1315.

(49) Liu, X.; Gao, K.; Li, Y.; Fu, J.; Wei, J.; Xie, S. Polaron Formation Dynamics in Conducting Polymers. *Synthetic metals* **2007**, *157*, 380–385.

(50) Li, Y.; Lagowski, J. B. Electric Field Effects on Bipolaron Transport in Heterocyclic Conjugated Polymers with Application to Polythiophene. *Optical Materials* **2010**, *32*, 1177–1187.